

Science

# Algorithm development for Martian atmospheric correction and spatiotemporal variation study of atmospheric profiles

Minqiang Zhu<sup>1,2</sup>, Hongjie Xie<sup>1</sup> and Huade Guan<sup>1,3</sup>

<sup>1</sup>Laboratory for Remote Sensing and Geoinformatics, Department of Geological Sciences, The University of Texas at San Antonio, Texas 78249 USA, [hongjie.xie@utsa.edu](mailto:hongjie.xie@utsa.edu); <sup>2</sup>Research Center for GIS and RS, East China Institute of Technology, Fuzhou, Jianxi 344000 China; <sup>3</sup>School of Chemistry, Physics and Earth Sciences, Flinders University, Adelaide 5001 Australia

**Citation:** Mars 5, 61-67, 2010; [doi:10.1555/mars.2010.0002](https://doi.org/10.1555/mars.2010.0002)

**History:** Submitted August 17, 2006; Reviewed: October 17, 2006; Revised; November 9, 2007; Reviewed: March 18, 2008; Revised: November 14, 2008; Accepted January 19, 2009; Published June 14, 2010

**Editor:** François Forget, Institut Pierre Simon Laplace

**Reviewers:** Yves Langevin, Institut d'Astrophysique Spatiale; Michael J. Wolff, Space Science Institute

**Open Access:** Copyright © 2010 Zhu et al. This is an open-access paper distributed under the terms of a [Creative Commons Attribution License](https://creativecommons.org/licenses/by/4.0/), which permits unrestricted use, distribution, and reproduction in any medium, provided the original work is properly cited.

---

## Abstract

**Background:** To identify minerals and other material at the surface of Mars using near infrared spectroscopy and hyperspectral imagery, a correction is necessary to take into account the effects of the atmosphere.

**Method:** A optional algorithm (including two logarithmic and two exponential calculations, or LLEE) for removing Martian atmospheric absorptions is developed, and compared with the existing empirical transmission function (ETF) method based on Olympus Mons.

**Conclusion:** LLEE only corrects prescribed atmospheric bands, thus exactly preserving the spectra other than the prescribed absorption bands. Besides the atmospheric correction, the LLEE algorithm can be used to study the temporal and spatial variation of Martian atmospheric profiles.

---

## Introduction

The OMEGA/Mars Express hyperspectral imagery of Mars provided by the European Space Agency (ESA), offers a great opportunity to study Martian surface materials and their spatial distributions with medium to coarse spatial resolutions (e.g., [Bibring et al. 2005](#); [Poulet et al. 2009](#)). The U.S. NASA CRISM (Compact Reconnaissance Imaging Spectrometers for Mars) launched in 2005 on board MRO (Mars Reconnaissance Orbiter) and has provided much higher spatial resolution (as fine as 18 meters) and spectral resolution (down to 6.55 nm) images of the Martian surface. Those images have confirmed many previous findings and also provided new information about the mineral/rock compositions of the Martian surface ([Murchie et al. 2007](#); [Mustard et al. 2008](#)). Atmospheric correction is required for the spectral imagery before it is used to identify surface minerals, rocks and other materials ([Resmini et al. 1997](#); [Clark et al. 2003](#); [Verhoef and Bach 2007](#)). With its dominant CO<sub>2</sub> composition ([Bibring et al. 1989](#)), the Martian atmospheric effect on the spectra of OMEGA (0.36-5.09 μm) and CRISM (0.38-3.96 μm) is characterized by several absorption bands of CO<sub>2</sub>. The trace gases' (e.g., H<sub>2</sub>O and CO) effect on this spectral region is not so significant,

though it may reach ~10% in absorption strength at 2.6 μm ([Encrenaz et al. 2005](#)). In addition to the effect of the gas components, aerosols in the atmosphere also alter the Martian surface spectra ([Blecka and Erard 2004](#)). The aerosols effect is characterized by strong silicate-induced absorption near 9 and 15 μm ([Forget 1998](#)), beyond the OMEGA and CRISM spectra. Aerosols can be significantly more hydrated than surface material. The major hydration bands lie between 2.7 and 3.6 μm, while they are spectrally relatively featureless between 0.95 to 2.6 μm, which is the main focus of this paper. A Monte Carlo approach was developed to model the aerosols effects on atmospherically corrected spectral reflectance of OMEGA imagery ([Vincendon et al. 2007](#); [Langevin et al. 2007](#)). Thus, removal of the CO<sub>2</sub> absorptions from the spectra is of great concern. In this paper, we focus on Martian atmospheric correction for the near infrared region (0.96-2.55 μm) of the OMEGA spectra, which is most useful for surface material identification.

Two atmospheric correction methods have been implemented to process the OMEGA data: band strength analysis ([Melchiorri et al. 2006](#)) and the empirical

transmission functions (ETF) method (Langevin et al. 2005). The ETF was originated by Bibring et al. (1989) and is the ratio ( $s_1/s_0$ ) of the reference spectra at the base of Olympus Mons ( $s_1$ ) and that at the top of Olympus Mons ( $s_0$ ). This ratio cancels out the reflectance of the surface materials (if they are radiometrically similar), and only leaves the apparent reflectance differences at the atmospheric absorption bands. This ratio curve is called the empirical transmission function,  $ETF = s_1/s_0$  (Combe et al. 2005). Ideally, the ETF should be exactly equal to 1 for the bands free of Martian atmospheric absorption. This result is achieved by carefully selecting spectrally homogeneous bright materials at both the top and bottom of the Olympus Mons. The ETF enables atmospheric correction of spectra ( $s$ ) of a pixel that has the same atmospheric optical depth of the ETF, by dividing  $s$  by the ETF. For simplicity, this procedure is referred to as the ETF method.

For an arbitrary spectral image, the atmospheric optical depth varies from pixel to pixel due to the elevation relief, and often is not equal to that of the reference ETF. Thus, the ETF should be re-scaled to the same atmospheric optical depth of the current pixels (Combe et al. 2005). This scaling is operationally achieved by applying a power  $x$  to ( $s_1/s_0$ ) so that the band depth at the 2.011  $\mu\text{m}$  (the biggest  $\text{CO}_2$  absorption in the spectral region we used) equals that of the pixel spectrum to be corrected. The ETF for the pixel spectrum to be corrected is ( $s_1/s_0$ ) <sup>$x$</sup> . The ETF curve is not available in the literature; users must construct the ETF curve based on their experience.

Because the ETF method is based on the reference spectra at the Olympus Mons, it does not correct the atmospheric absorption at locations where the atmospheric column is far thicker than the reference location. The ETF method does not work well for locations with very low elevation such as those in Hellas (-7 km). Also, the ETF method neglects the difference in surface spectral reflectance between the base and the summit of the Olympus Mons; it slightly alters the spectra for the bands free of atmospheric absorption. We thus develop an optional approach including two logarithmic and two exponential calculations (or LLEE) to correct Martian atmospheric effect. A comparison of the LLEE with the ETF method is also made. The LLEE approach directly removes  $\text{CO}_2$  absorptions based on the target image itself. It does not require reference spectra at the Olympus Mons. Also, this method exactly preserves the spectra free of Martian atmospheric absorptions. A brief description of these developments first appeared in Guan et al. (2006).

## Algorithm development

We started from a simple radiative transfer function, only considering Martian atmospheric  $\text{CO}_2$  absorption. For an arbitrary pixel, following Beer's law, we have

$$I_\lambda = F_\lambda r e^{\tau_\lambda}, \quad (1)$$

where  $I$  is the upward spectral radiance intensity of the  $\text{CO}_2$  absorption band ( $\lambda$ ) at the remote sensor,  $F$  is the downward

spectral radiance intensity at the top of Martian atmosphere,  $r$  is the bidirectional spectral reflectance of the ground surface,  $\tau$  is the two-way spectral optical depth of the local Martian atmospheric  $\text{CO}_2$  along the radiation path from incoming radiation at the top of the atmosphere to outgoing radiation at the remote sensor, which is a function of the number of  $\text{CO}_2$  molecules in the path and the ability of the  $\text{CO}_2$  to absorb the photons of wavelength in question (opacity) (Tennyson 2005). For a spectral band where it is free of  $\text{CO}_2$  absorption,  $\tau$  is zero. For a specific absorption band, it is reasonable to assume that the spectral reflectance of the surface is the same as that of the neighboring bands. Thus, the ratio of  $I/F$  value between a  $\text{CO}_2$  absorption band and the continuum obtained from the neighboring bands without  $\text{CO}_2$  absorption is

$$\frac{(I/F)_\lambda}{(I/F)_{\bar{\lambda}}} = \frac{r e^{\tau_\lambda}}{r} = e^{\tau_\lambda}, \quad (2)$$

where  $(I/F)_\lambda$  is the  $I/F$  value at a specific  $\text{CO}_2$  absorption band  $\lambda$ ,  $(I/F)_{\bar{\lambda}}$  is the continuum at the same  $\text{CO}_2$  absorption band  $\bar{\lambda}$ , calculated from the neighboring bands without suffering  $\text{CO}_2$  absorption. These spectral  $I/F$  values are directly obtained from the spectral imagery (e.g., OMEGA).

Our objective is to remove the  $\text{CO}_2$  absorption effect from  $(I/F)_\lambda$ . However, we cannot directly use (2) to correct for all  $\text{CO}_2$  absorption bands because  $(I/F)_\lambda$  may also include the contributions of ground surface absorption or other gases such as water vapor. These contributions at different bands are of great value to the study of the surface characteristics of Mars, and are the primary motivation for doing atmospheric correction.

The  $\text{CO}_2$  optical depth at individual absorption wavelength (band) is a function of both physical  $\text{CO}_2$  column density (vertical profile) and wavelength-dependent opacity. The optical depth also depends on the radiative transfer path, which is a function of solar incident angle and sensor viewing angle. For a small scene of a relative flat surface, the radiative transfer path is similar among the pixels. This is clearly observed from the elevation versus optical-depth plots at different bands of the OMEGA scene at the Olympus Mons (Figure 1). In this figure, the optical depth was calculated according to Equation (2). The similar shape of data clouds between the two selected  $\text{CO}_2$  absorption bands indicates the common effects of  $\text{CO}_2$  vertical profile (or column density), while the different values of optical depth indicate the different opacity at the two bands: a much larger opacity at 2.011  $\mu\text{m}$  (left) than at 1.601  $\mu\text{m}$  (right). For both bands, the optical depth at the top of Olympus Mons is still  $\sim 10\%$  of that at the base of the Mons. The effect of the physical  $\text{CO}_2$  profile is fixed for one arbitrary pixel, which can be obtained from the spectral of  $\text{CO}_2$  absorption band at 2.011  $\mu\text{m}$ . At this band, the  $\text{CO}_2$  absorption is so large that the spectral contribution from the ground surface is negligible. To transfer this  $\text{CO}_2$  vertical profile for calculating optical depths at other  $\text{CO}_2$  absorption bands, we need to explicitly separate the two components in the optical

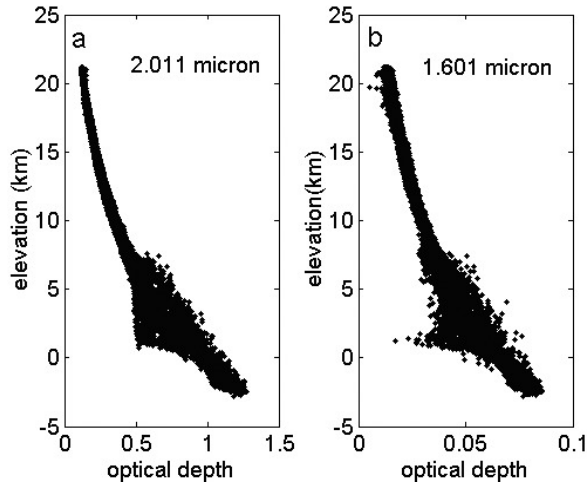


**Figure 1.** The scatter plots of pixel optical depths ( $\tau_\lambda$ , calculated from equation (2) vs. pixel elevations for two CO<sub>2</sub> absorption bands: left = 2.011  $\mu\text{m}$  (**a**), right = 1.601  $\mu\text{m}$  (**b**), derived from OMEGA (ORB0501-4) spectra at the Olympus Mons, showing exponential decay of the optical depth with elevation. The scattering points away from the exponential curve are those on the steep slopes or shadow of cliff of the Olympus Mons ([figure1.jpg](#)).

depth: the CO<sub>2</sub> column density and the wavelength-dependent opacity.

According to the shape of the optical depth vs. elevation plots (Figure 1), we assume that  $\tau_\lambda$  is an exponential function of elevation  $z$ , as shown in Equation (3). From this, we decompose the optical depth into two components: one depending on CO<sub>2</sub> absorption-induced opacity and CO<sub>2</sub> column density above Martian zero elevation surface (or MOLA  $z = 0$ ), and the other only depending on the atmospheric vertical profile of CO<sub>2</sub> column density.

$$\tau_\lambda = Ae^{-kz}, \quad (3)$$

where  $A$  is the optical depth for the wavelength of interest at the zero elevation surface and depends on CO<sub>2</sub> absorption characteristics of different bands and the CO<sub>2</sub> column density above  $z = 0$ ,  $z$  is the MOLA elevation in the Martian atmospheric column, and  $k$  is a factor only depending on the vertical profile of the Martian atmospheric column, considered a constant for one scene with a small latitude range (e.g., 10-20°). From (2) and (3), we have

$$\log\left(-\log\left(\frac{(I/F)_\lambda}{(I/F)_\lambda^0}\right)\right) = \log(\tau_\lambda) = \log(A) - kz. \quad (4)$$

If our assumption for  $\tau$  in equation (3) is valid, the plot of  $\log(\tau_\lambda)$  with elevation should be a straight line with a slope of  $-k$  and an interception of  $\log A$ . This is evident from the plots of  $\log(\tau_\lambda)$  vs.  $z$  for the 2.011  $\mu\text{m}$  CO<sub>2</sub> absorption bands of two OMEGA images at Olympus Mons and one OMEGA image at the Ascræus Mons (Figure 2). This exponential relationship between optical depth and elevation on Mars is

different from that on Earth (e.g., [Clark et al. 2003](#)), probably because CO<sub>2</sub> is the predominant component on Mars, while it is a trace atmospheric component on Earth. For the two images of the Olympus Mons taken at different seasons, the  $A$  value at the same CO<sub>2</sub> absorption band is slightly different, indicating slightly different CO<sub>2</sub> column density at MOLA zero surface between the two seasons. The  $k$  value varies between the two because the physical CO<sub>2</sub> column vertical profile changes between seasons. For the two images (ORB0501-4 and ORB0519-4) taken at the same season but different areas (latitude), both  $A$  and  $k$  are significantly different.

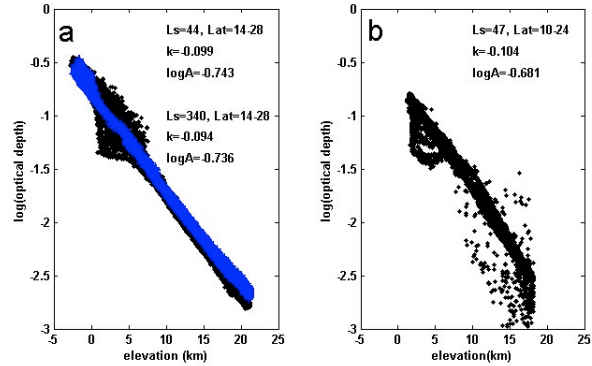


**Figure 2.** The scatter plots of the natural log of optical depth ( $\tau_\lambda$ ) vs. pixel elevations for the CO<sub>2</sub> absorption band (2.011  $\mu\text{m}$ ), derived from OMEGA images (ORB0501-4,  $L_s = 44^\circ$ , latitude = 14~28° and ORB0037-3,  $L_s = 340^\circ$ , latitude = 14~28°, pixels with latitude over 28 were omitted) at the Olympus Mons (**a**), and OMEGA image (ORB0519-4,  $L_s = 47^\circ$ , latitude = 10~24°) at the Ascræus Mons (**b**), and the inferred  $k$  and  $\log A$  values from the linear regressions. The scattering points away from the linear trend are due to steep slopes or shadow of cliff of the Olympus Mons for the scenes ORB0501-4 and ORB0037-3, and bad lines for the scene ORB0519-4 ([figure2.jpg](#)).

Different CO<sub>2</sub> absorption bands in one OMEGA image should have the same  $k$  values because they share one vertical atmospheric profile, but different  $A$  values because of different opacity between the bands. This is evident from the parallel patterns of the

$$\log\left(-\log\left(\frac{(I/F)_\lambda}{(I/F)_\lambda^0}\right)\right),$$

or  $LL$  hereafter, plot of various Martian atmospheric absorption bands at various elevations of the OMEGA scene (ORB0501-4) (Figure 3). On the  $LL$  plot, the difference between any two elevations at one CO<sub>2</sub> absorption band is the same as any other CO<sub>2</sub> absorption band, i.e.,  $k(z_2 - z_1)$ , leading to parallel patterns. If we adjust the elevation  $z$  to a certain threshold height in the Martian atmosphere above which CO<sub>2</sub> absorption is negligible, the Martian atmospheric effects can then be removed. Operationally, let  $LL_0$  be  $\log(A) - kz$  for the carbon dioxide absorption band (2.011  $\mu\text{m}$ ) at this threshold height. The difference between

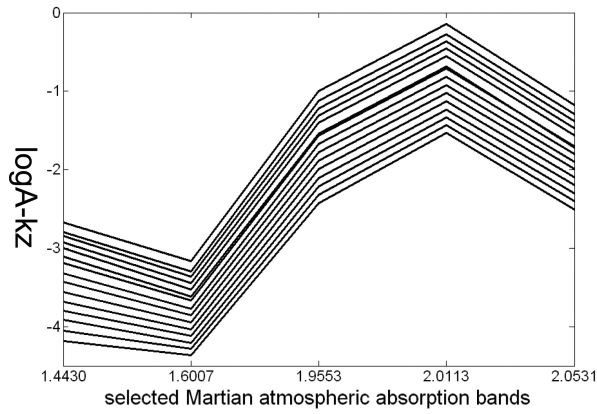


**Figure 3.** Calculated values of  $LL$  (equal to  $\log A - kz$ ) for 5 selected absorption bands over 15 1km-elevation intervals between 0-15 km of average OMEGA (ORB0501-4) spectra in the Olympus Mons, with lines ordered from the top to the bottom corresponding to from the lowest to the highest elevation of the selected elevations ranges. The parallel patterns of the atmospherically associated absorption bands at various elevations are clearly observed ([figure3.jpg](#)).

pixel  $LL$  and  $LL_0$  at 2.011  $\mu\text{m}$  is given by

$$\Delta = \left[ \log \left( -\log \left( \frac{(I/F)_\lambda}{(I/F)_\bar{\lambda}} \right) \right) - LL_0 \right]_{@2.011\mu\text{m}} \quad (5)$$

The value of  $\Delta$  is then subtracted from  $LL$  for all atmospheric ( $\text{CO}_2$ ) absorption bands, as given by

$$LL' = LL - \Delta. \quad (6)$$

The corrected  $LL$  values ( $LL'$ ) after equation (6) can be used to generate final atmospherically corrected  $I/F$  for Martian spectral images, as shown in equation (7),

$$(I/F)_\lambda' = \exp(-\exp(LL')) (I/F)_\bar{\lambda}. \quad (7)$$

The above procedure includes two logarithmic and two exponential calculations. For simplicity, we refer to this approach as the LLEE method. The LLEE method is applied with a carefully prescribed  $LL_0$  to remove the Martian atmospheric absorption effect. If  $LL_0$  is too big, the Martian atmospheric absorption is not removed completely. If it is too small, the atmospheric absorption is over-corrected, and the absorption contributions from the Martian surface may be underestimated. We estimate  $LL_0$  to be -4.6, equivalent to 1/10  $\text{CO}_2$  optical depth at the top of the Olympus Mons. When this is determined, the algorithm is implemented based on the target image itself and does not require reference curves for correction. The LLEE calculations are only conducted on the prescribed atmospheric absorption bands. Table 1 lists the prescribed absorption bands and continuum used for the algorithm. The major  $\text{CO}_2$  absorption bands are 1.4430, 1.6007, and 2.0113  $\mu\text{m}$ . The major atmospheric  $\text{H}_2\text{O}$  absorption band used in the range is 1.8709  $\mu\text{m}$ . The remaining bands are selected based on our experience examining the ETF ( $s_1/s_0$ ) spectra. It should be

noticed that this table is by no means an exhaustive list of all atmospheric gases absorptions, and it can be easily added to or modified based on a better understanding of the Martian atmospheric absorptions.

**Table 1.** Atmospheric absorption bands and continuum used for the LLEE algorithm.

Absorption bands		Continuum used	
Band	Wavelength ( $\mu\text{m}$ )	Band	Wavelength ( $\mu\text{m}$ )
		126	1.3424
132	1.4286	Interpolation between band 126 and band 138	
133	1.4430		
		138	1.5148
142	1.5721		
143	1.5884	Interpolation between band 138 and band 150	
144	1.6007		
145	1.6150		
		150	1.6864
		162	1.8568
163	1.8709	Directly uses 162	
164	1.8850		
168	1.9413		
169	1.9553		
170	1.9693		
171	1.9834		
172	1.9973		
173	2.0113	Interpolation between band 162 and band 182	
174	2.0253		
175	2.0392		
176	2.0531		
177	2.0670		
178	2.0809		
179	2.0948		
180	2.1087		
		182	2.1363

### Algorithm testing

We implemented the LLEE algorithm (available upon request) using the Modeler Builder of ERDAS IMAGINE, a commercial image processing software program. The algorithm was tested with four selected pixels of various latitudes, elevations, seasons and albedo, and compared with the ETF algorithm-corrected spectra (Y. Langevin kindly provided the algorithm) (Figure 4). Overall, while apparent over-corrections or under-corrections at the 2.011  $\mu\text{m}$  are clearly seen in the ETF spectra (Figure 4a,b,c), the LLEE corrected spectra are similar to those corrected by the ETF method. For example, the water ice absorption at 1.5  $\mu\text{m}$  is clear in both LLEE and ETF corrected curves (Figure 4b). In the Hellas crater (ORB0030-1, Figure 4c), the low altitude (-7.2 km) results in large atmospheric depths which could create problems for the ETF method; the LLEE method, however, is effective in removing the larger atmospheric absorption. A clear gypsum signature was detected by the ETF method ([Langevin et al. 2005](#)). Here, we use the ORB0942\_2 image to test the LLEE algorithm. A 27% absorption depth at 1.927  $\mu\text{m}$  is detected by both the LLEE and ETF methods (Figure 4d). Other absorption features of gypsum (1.45, 1.75, 1.94, 2.22, 2.26, and 2.48  $\mu\text{m}$ ) are also very clear and have very similar absorption depths in both

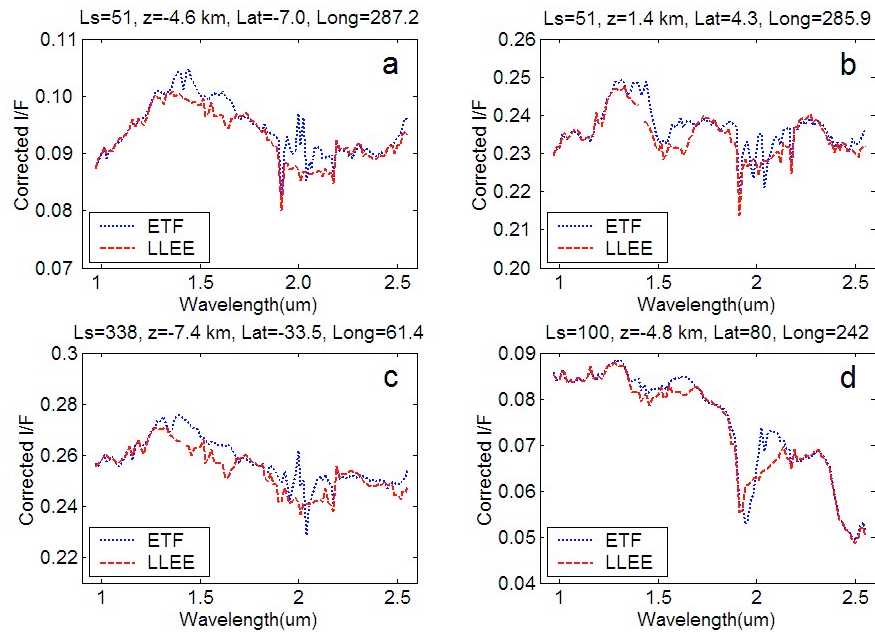


**Figure 4.** The ETF and LLEE corrected OMEGA spectra for four selected pixel with various latitudes, seasons, elevations, and albedo: (a) ORB0548-3; (b) ORB0548-3; (c) ORB0030-1; (d) ORB0942\_2 ([figure4.jpg](#)).

spectra, except at  $1.94 \mu\text{m}$ . The absorption depth at  $1.94 \mu\text{m}$  is 32% from the ETF spectrum and 21% from the LLEE spectrum. In the paper by [Langevin et al. \(2005\)](#), the  $1.927 \mu\text{m}$  band was used rather than the  $1.94 \mu\text{m}$  band for measuring the absorption depth, since atmospheric  $\text{CO}_2$  absorption is much small at  $1.927 \mu\text{m}$  than at  $1.94 \mu\text{m}$ . The LLEE algorithm may overcorrect the  $\text{CO}_2$  absorption at the  $1.94 \mu\text{m}$  band. In addition, the LLEE algorithm fails in recovering the higher reflectivity at the  $2.05 \mu\text{m}$ , an obvious peak at the EFT spectrum. This failure (assuming the ETF method is the right one) can be explained by examining Table 1, in which a total of 16 bands between  $1.8568 \mu\text{m}$  and  $2.1363 \mu\text{m}$  used the same two bands for continuum calculation through interpolation. Thus, the maximum reflectivity of those 16 bands after the LLEE correction should be always between the reflectivity values at  $1.8568 \mu\text{m}$  and  $2.1363 \mu\text{m}$ . If a mineral or rock has a reflectivity value (peak) higher than the continuum based on reflectivity values at  $1.8568 \mu\text{m}$  and  $2.1363 \mu\text{m}$ , the LLEE method will not be able to correctly recover the peak value.

## Discussion

The LLEE method corrects the  $\text{CO}_2$  absorption for the prescribed bands and requires the continuum for each individual absorption band. The biggest advantage of the LLEE method is that it does not require the reference spectra of the Olympus Mons. Thus, it has the capacity to completely remove  $\text{CO}_2$  absorption. Its performance is independent of latitudes and elevations of the images. Also, the LLEE method does not alter the spectra of bands free of  $\text{CO}_2$  absorption. However, there are limitations of the LLEE method. For example, in the gypsum case above, it is found that LLEE overcorrects the  $\text{CO}_2$  absorption at  $1.94 \mu\text{m}$  and

does not recover a reflectivity value (at  $2.05 \mu\text{m}$ ) larger than the continuum based on reflectivity values at  $1.8568 \mu\text{m}$  and  $2.1363 \mu\text{m}$ . The described bands in Table 1 are critical to the success of the LLEE algorithm and should be improved as our understanding of Martian atmospheric absorption bands improves.

In addition to Martian atmospheric correction, the LLEE method can be used to study the temporal and spatial variability of the atmospheric  $\text{CO}_2$  profile and column density. The LLEE algorithm separates the atmospheric absorption into two factors. The first factor is represented by the  $A$  term, and the second factor by the  $kz$  term in Equation (4). The value of  $A$  is a function of  $\text{CO}_2$ -induced opacity and the  $\text{CO}_2$  column density above the Martian zero elevation surface, and it should be a constant for a specific absorption band in one image scene with a small latitude range, while varying in different absorption bands. The value of  $k$  represents the effect of the vertical profile of  $\text{CO}_2$  column density in Martian atmosphere. For a similar Martian atmospheric vertical profile (*e.g.*, in one scene),  $k$  should be similar.

When the Martian atmospheric column changes with time and location (*e.g.*, because of Martian global  $\text{CO}_2$  circulation), the  $k$  and  $A$  values change accordingly (Figure 2). Thus, both  $k$  and  $A$  can be used as indicators of Martian atmospheric column variation, which can be derived from any Martian spectral image with a certain topographic relief. If the temperature effect on  $\text{CO}_2$  absorption (*i.e.*, opacity, lumped in  $A$  term) is negligible at the temperature range of Martian atmosphere, both  $A$  and  $k$  can be used to inform  $\text{CO}_2$  column density variation on Mars.

## Conclusions

This paper presents an optional algorithm (LLEE) for removing Martian CO<sub>2</sub> absorptions. The LLEE method only corrects prescribed atmospheric bands, and exactly preserves spectra other than the prescribed bands. In addition to the atmospheric correction, the LLEE method can be used to study the temporal and spatial CO<sub>2</sub> variation of the Martian atmosphere. The disadvantage of the LLEE method is that each atmospheric absorption band and continuum must be identified. However, once well defined, they can be used for any image.

## Directory of supporting data

[root directory](#)

[zhu mars 2010 0002.pdf](#)

Fig. 1 [figure1.jpg](#) full-resolution image

Fig. 2 [figure2.jpg](#) full-resolution image

Fig. 3 [figure3.jpg](#) full-resolution image

Fig. 4 [figure4.jpg](#) full-resolution image

## Acknowledgements

The authors would like to thank Yves Langevin, John Mustard and Joe Zender for their directions on the OMEGA data pre-processing. Kind description of the ETF algorithm from Yves Langevin, Aline Gendrin and John Mustard, is greatly appreciated. M. Zhu would like to thank the Chinese State Scholarship Fund Award (2005-2006) for making this collaborative study possible. The project is partly supported by a NASA/Texas Space Grant Consortium New Investigations Program (#NNG05GE96H).

## References

- Bibring, J.P., M. Combes, Y. Langevin, A. Soufflot, C. Cara, P. Drossart, Th. Encrenaz, S. Erard, O. Forni, B. Gondet, L. Ksanfomalft, E. Lellouch, Ph. Masson, V. Moroz, F. Rocard, J. Rosenqvist and C. Sotin (1989) "Results from the ISM experiment" *Nature* 341, 591-593. [doi:10.1038/341591a0](#)
- Bibring, J. P., Y. Langevin, A. Gendrin, B. Gondet, F. Poulet, M. Berthé, A. Soufflot, R. Arvidson, N. Mangold, J. Mustard, P. Drossart and the OMEGA team (2005) "Mars surface diversity as revealed by the OMEGA/Mars Express observations" *Science* 307, 1576-1581. [doi:10.1126/science.1108806](#)
- Blecka, M. I. and S. Erard (2004) "Numerical simulation of the visible and near infrared radiance of Mars: effects of atmospheric scattering, Planetary Ionospheres and Atmospheres Including CIRA" *Advances in Space Research* 34, 1683-1689. [doi:10.1016/j.asr.2003.07.075](#)
- Clark, R. N., G. A. Swayze, K. E. Livo, R. F. Kokaly, S. J. Sutley, J. B. Dalton, R. R. McDougal and C. A. Gent (2003) "Imaging spectroscopy: Earth and planetary remote sensing with the USGS Tetracorder and expert systems" *Journal of Geophysical Research* 108, 5131. [doi:10.1029/2002JE001847](#)
- Combe, J-Ph., C. Sotin, S. L. Mouélic, P. Launeau, J. Mustard, A. Gendrin, J. P. Bibring, B. Gondet, Y. Langevin and the OMEGA Science team (2005) "Methodology of spectral reflectance data analysis for mineralogical mapping of planetary surface: application to OMEGA/Mars - Express images" 36<sup>th</sup>

- Lunar and Planetary Science Conference, Abstract No. 1633, League City, Texas.
- Guan, H., H. Xie and M. Zhu (2006) "Development of an alternative Martian atmospheric correction algorithm for OMEGA/Mars Express imagery" 37<sup>th</sup> Lunar and Planetary Science Conference, Abstract No. 1934, League City, Texas.
- Encrenaz, T., R. Melchiorri, T. Fouchet, P. Drossart, E. Lellouch, B. Gondet, J. P. Bibring, Y. Langevin, D. Titov, N. Ignatiev and F. Forget (2005) "A mapping of martian water sublimation during early northern summer using OMEGA/Mars Express" *Astronomy and Astrophysics* 441(3), 9-12. [doi:10.1051/0004-6361:200500171](#)
- Forget, F. (1998) "Improved optical properties of the Martian atmospheric dust for radiative transfer calculations in the infrared" *Geophysical Research Letters* 25(7), 1105-1108. [doi:10.1029/98GL50653](#)
- Langevin, Y., F. Poulet, J. P. Bibring and B. Gondet (2005) "Sulfates in the north polar region of Mars detected by OMEGA/Mars Express" *Science* 307, 1584-1586. [doi:10.1126/science.1109091](#)
- Langevin, Y., J. P. Bibring, F. Montmessin, F. Forget, M. Vincendon, S. Doute', F. Poulet and B. Gondet (2007) "Observations of the south seasonal cap of Mars during recession in 2004-2006 by the OMEGA visible/near-infrared imaging spectrometer on board Mars Express" *Journal of Geophysical Research* 112, E08S12. [doi:10.1029/2006JE002841](#)
- Melchiorri, R., P. Drossart, T. Fouchet, B. Bezard, F. Forget, A. Gendrin, J. P. Bibring, N. Manaud and the OMEGA team (2006) "A simulation of the OMEGA/Mars Express observations: analysis of the atmospheric contribution" *Planetary and Space Science* 54, 774-783. [doi:10.1016/j.pss.2006.04.014](#)
- Murchie, S. et al. (2007) "Compact Reconnaissance Imaging Spectrometer for Mars (CRISM) on Mars Reconnaissance Orbiter (MRO)" *Journal of Geophysical Research* 112, E05S03. [doi:10.1029/2006JE002682](#)
- Mustard, J. F., S. L. Murchie, S. M. Pelkey, B. L. Ehlmann, R. E. Milliken, J. A. Grant, J.-P. Bibring, F. Poulet, J. L. Bishop, E. Z. Noe Dobrea, L. H. Roach, F. P. Seelos, R. E. Arvidson, S. Wiseman, R. Green, C. Hash, D. Humm, E. Malaret, J. A. McGovern, Y. Langevin, T. Martin, P. McGuire, R. Morris, M. S. Robinson, T. Roush, M. Smith, G. Swayze, H. Taylor and M. Wolf (2008) "Hydrated silicate minerals on Mars observed by the Mars Reconnaissance Orbiter CRISM instrument" *Nature* 454, 305-309. [doi:10.1038/nature07097](#)
- Poulet, F., N. Mangold, B. Platevoet, J.-M. Bardintzeff, V. Sautter, J. F. Mustard, J.-P. Bibring, P. C. Pinet, Y. Langevin, B. Gondet and A. Aléon-Toppani (2009) "Quantitative compositional analysis of martian mafic refions using the MEx/OMEGA reflectance data 2. Petrological implications" *Icarus* 201, 84-101. [doi:10.1016/j.icarus.2008.12.042](#)
- Resmini, R. G., M. E. Kappus, W. S. Aldrich, J. C. Harsanyi and M. Anderson (1997) "Mineral mapping with spectral digital imagery collection experiment (HYDICE) sensor data at Cuprite, Nevada, U.S.A." *International Journal of Remote Sensing* 18, 1553-1570. [doi:10.1080/014311697218278](#)
- Tennyson, J. (2005) "Astronomical Spectroscopy: An Introduction to the Atomic and Molecular Physics of Astronomical Spectra" Imperial College Press, London.
- Verhoef, W. and H. Bach (2007) "Coupled soil-leaf-canopy and atmosphere radiative transfer modeling to simulate spectral multi-angular surface reflectance and TOA radiance data" *Remote Sensing of*

Environment, 109, 166-182.

[doi:10.1016/j.rse.2006.12.013](https://doi.org/10.1016/j.rse.2006.12.013)

Vincendon, M., Y. Langevin, F. Poulet, J.-P. Bibring and B. Gondet (2007) "Recovery of surface reflectance spectra and evaluation of the optical depth of aerosols in the near-IR using a Monte Carlo approach: Application to the OMEGA observations of high-latitude regions of Mars" Journal of Geophysical Research 112, E08S13. [doi:10.1029/2006JE002845](https://doi.org/10.1029/2006JE002845)